

Supplementary Material to Synchronization and temporal nonreciprocity of optical microresonators via spontaneous symmetry breaking

Da Xu^{1,2}, Zi-Zhao Han¹, Yu-Kun Lu¹, Qihuang Gong^{1,2,3}, Cheng-Wei Qiu⁴, Gang Chen^{2,5,*} and Yun-Feng Xiao^{1,2,3†}

¹*State Key Laboratory for Mesoscopic Physics and Collaborative Innovation Center of Quantum Matter,
School of Physics, Peking University, Beijing 100871, People's Republic of China*

²*Collaborative Innovation Center of Extreme Optics,
Shanxi University, Taiyuan 030006, People's Republic of China*

³*Department of Electrical and Computer Engineering,
National University of Singapore, Singapore 117576, Singapore*

⁴*Beijing Academy of Quantum Information Sciences, Beijing 100193, People's Republic of China and*

⁵*State Key Laboratory of Quantum Optics and Quantum Optics Devices,
Institute of Laser Spectroscopy, Shanxi University, Taiyuan 030006, People's Republic of China*

(Dated: July 31, 2019)

This Supplemental Material is organized as follows. In Sec. **I**, the mode equations in the main text are derived, with the analytical form of drift flow terms and the noise terms. In Sec. **II**, the trajectories and topologies for the different long-term states are analyzed in the transformed space, revealing two different topological structures. In Sec. **III**, the noisy response of the system is calculated in long-term and the exact noise resonance frequencies are specified. In Sec. **IV**, the dynamical potential is defined and the derivation of different types of synchronization transitions is presented. In Sec. **V**, the emergence of the hysteresis loop is explained by means of a perturbative analysis. The symbols used in this material share the same meaning with those in the main text.

I. DERIVATIONS OF MODE EQUATIONS

The dissipative evolution of the system is described by the Lindblad density-matrix equation ($\hbar = 1$ hereafter),

$$\dot{\rho} = -i[H, \rho] + \sum_{j=1,2} \left(G_j \mathcal{D}[a_j^\dagger] \rho + \frac{R_j}{2} \mathcal{D}[a_j^2] \rho \right), \quad (\text{S1})$$

$$H = \sum_{j=1,2} \left[\omega_{j0} a_j^\dagger a_j + \frac{1}{2} \delta_j (a_j^\dagger a_j)^2 \right] + g(a_2^\dagger a_1 + a_1^\dagger a_2), \quad (\text{S2})$$

where $\mathcal{D}[o]\rho = 2o\rho o^\dagger - o^\dagger o\rho - \rho o^\dagger o$. By setting $R_1 = R_2 = R > 0$, $G_1 = G_2 = G > 0$ and $\delta_1 = \delta_2 = \delta > 0$, the evolution of the Wigner function in the coherent-state representation is written as

$$\begin{aligned} \frac{d}{dt} W(\alpha_1, \alpha_2, \bar{\alpha}_1, \bar{\alpha}_2) = & \left\{ i(\Delta\alpha_1 + \delta|\alpha_1|^2\alpha_1 + g\alpha_2)\partial_{\alpha_1} + i(\delta|\alpha_2|^2\alpha_2 + g\alpha_1)\partial_{\alpha_2} - \right. \\ & i(\Delta\bar{\alpha}_1 + \delta|\alpha_1|^2\bar{\alpha}_1 + g\bar{\alpha}_2)\partial_{\alpha_1} - i(\delta|\alpha_2|^2\bar{\alpha}_2 + g\bar{\alpha}_1)\partial_{\bar{\alpha}_2} + \\ & \sum_{j=1,2} 2G \left[\left(\alpha_j - \frac{1}{2}\partial_{\bar{\alpha}_j} \right) \left(\bar{\alpha}_j - \frac{1}{2}\partial_{\alpha_j} \right) - \frac{1}{2} \left(\alpha_j - \frac{1}{2}\partial_{\bar{\alpha}_j} \right) \left(\bar{\alpha}_j + \frac{1}{2}\partial_{\alpha_j} \right) - \frac{1}{2} \left(\alpha_j + \frac{1}{2}\partial_{\bar{\alpha}_j} \right) \left(\bar{\alpha}_j - \frac{1}{2}\partial_{\alpha_j} \right) \right] + \\ & \sum_{j=1,2} R \left[\left(\bar{\alpha}_j^2 + \bar{\alpha}_j \partial_{\alpha_j} + \frac{1}{4} \partial_{\alpha_j}^2 \right) \left(\alpha_j^2 + \alpha_j \partial_{\bar{\alpha}_j} + \frac{1}{4} \partial_{\bar{\alpha}_j}^2 \right) - \frac{1}{2} \left(\bar{\alpha}_j^2 - \bar{\alpha}_j \partial_{\alpha_j} + \frac{1}{4} \partial_{\alpha_j}^2 \right) \left(\alpha_j^2 + \alpha_j \partial_{\bar{\alpha}_j} + \frac{1}{4} \partial_{\bar{\alpha}_j}^2 \right) - \right. \\ & \left. \frac{1}{2} \left(\alpha_j^2 - \alpha_j \partial_{\bar{\alpha}_j} + \frac{1}{4} \partial_{\bar{\alpha}_j}^2 \right) \left(\bar{\alpha}_j^2 + \bar{\alpha}_j \partial_{\alpha_j} + \frac{1}{4} \partial_{\alpha_j}^2 \right) \right] \left. \right\} W(\alpha_1, \alpha_2, \bar{\alpha}_1, \bar{\alpha}_2). \quad (\text{S3}) \end{aligned}$$

*Electronic address: chengang971@163.com

†Electronic address: yfxiao@pku.edu.cn; URL: www.phy.pku.edu.cn/~yfxiao/

By further defining $\mathbf{\Lambda} = (\alpha_1, \alpha_2)$, Eq. (S3) is rewritten as a neat form

$$\frac{d}{dt}W(\mathbf{\Lambda}, \bar{\mathbf{\Lambda}}) = -\mathbf{f}(\mathbf{\Lambda}, \bar{\mathbf{\Lambda}}) \cdot \nabla W(\mathbf{\Lambda}, \bar{\mathbf{\Lambda}}) + \underbrace{\mathbf{D}(\mathbf{\Lambda}, \bar{\mathbf{\Lambda}}) : \nabla \nabla W(\mathbf{\Lambda}, \bar{\mathbf{\Lambda}})}_{\text{Noise terms}} + \frac{R}{8}(\mathbf{\Lambda}, \bar{\mathbf{\Lambda}})^\top \cdot \nabla \nabla^\dagger \cdot \nabla W(\mathbf{\Lambda}, \bar{\mathbf{\Lambda}}), \quad (\text{S4})$$

where $\nabla = (\partial_{\alpha_1}, \partial_{\alpha_2}, \partial_{\bar{\alpha}_1}, \partial_{\bar{\alpha}_2})^\top$, the drift flow function

$$\mathbf{f}(\mathbf{\Lambda}, \bar{\mathbf{\Lambda}}) = \begin{pmatrix} (G + R - i\Delta)\alpha_1 - (R + i\delta)|\alpha_1|^2\alpha_1 - ig\alpha_2 \\ (G + R)\alpha_2 - (R + i\delta)|\alpha_2|^2\alpha_2 - ig\alpha_1 \\ (G + R + i\Delta)\bar{\alpha}_1 - (R - i\delta)|\alpha_1|^2\bar{\alpha}_1 + ig\bar{\alpha}_2 \\ (G + R)\bar{\alpha}_2 - (R - i\delta)|\alpha_2|^2\bar{\alpha}_2 + ig\bar{\alpha}_1 \end{pmatrix}, \quad (\text{S5})$$

and the diffusion matrix

$$\mathbf{D}(\mathbf{\Lambda}, \bar{\mathbf{\Lambda}}) = \begin{pmatrix} 0 & 0 & \frac{G-R}{2} + R|\alpha_1|^2 & 0 \\ 0 & 0 & 0 & \frac{G-R}{2} + R|\alpha_2|^2 \\ \frac{G-R}{2} + R|\alpha_1|^2 & 0 & 0 & 0 \\ 0 & \frac{G-R}{2} + R|\alpha_2|^2 & 0 & 0 \end{pmatrix}. \quad (\text{S6})$$

Under the rescaled time $\tau = Gt$, the first linear drift term of the right part in Eq. (S4) is invariant under the scale transformation $\alpha_j \rightarrow A\alpha_j$ with $A = \sqrt{G/R}$, while its second and third noise terms are of A^{-2} and A^{-4} . Typically, the photon number is extremely large in a lasing system with $A^2 \gg 1$, so that the second and third noise terms can be eliminated. Here the nonlinear noise terms gives the analytical formula in Eq. (2) in the main text. The linear drift term portrays explicit trajectories in the phase space [S1].

In order to explore the effect induced by the drift term, a Dirac delta function is set to be the initial condition, i.e.,

$$\frac{d}{dt}W(\mathbf{\Lambda}', \bar{\mathbf{\Lambda}}') = -\mathbf{f}(\mathbf{\Lambda}', \bar{\mathbf{\Lambda}}) \cdot \nabla' W(\mathbf{\Lambda}', \bar{\mathbf{\Lambda}}'), \quad (\text{S7})$$

$$W(\mathbf{\Lambda}', \bar{\mathbf{\Lambda}}')|_{t=0} = \delta(\mathbf{\Lambda}' - \mathbf{\Lambda}, \bar{\mathbf{\Lambda}}' - \bar{\mathbf{\Lambda}}). \quad (\text{S8})$$

The solution of Eq. (S7) is still a delta function $\delta(\mathbf{\Lambda}' - \mathbf{\Lambda}(t), \bar{\mathbf{\Lambda}}' - \bar{\mathbf{\Lambda}}(t))$ with a moving center $\mathbf{\Lambda}(t)$, whose evolution equation is given by

$$(\dot{\mathbf{\Lambda}}, \dot{\bar{\mathbf{\Lambda}}})^\top = \mathbf{f}(\mathbf{\Lambda}, \bar{\mathbf{\Lambda}}). \quad (\text{S9})$$

Substituting the parametric form, $\alpha_j = Ar_j e^{i\phi_j}$, into Eq. (S9) yields

$$\dot{r}_1 = -r_1^3 + r_1 - \tilde{g}r_2 \sin(\phi), \quad (\text{S10})$$

$$\dot{r}_2 = -r_2^3 + r_2 + \tilde{g}r_1 \sin(\phi), \quad (\text{S11})$$

$$\dot{\phi} = -\tilde{\Delta} - \tilde{\delta}(r_1^2 - r_2^2) - \tilde{g} \frac{r_2^2 - r_1^2}{r_1 r_2} \cos(\phi), \quad (\text{S12})$$

where $\tilde{\delta} = \delta/R$, $\tilde{\Delta} = (\omega_{10} - \omega_{20})/G$, $\tilde{g} = g/G$ and $\tau = Gt$ are the dimensionless parameters. Based on Eqs. (S10)-(S12), three different long-term evolutions can be calculated, as shown in Fig. 2 of the main text.

II. TRAJECTORIES AND TOPOLOGIES

In the main text, the synchronized, limit cycle and unsynchronized states have been demonstrated in the light of Eqs. (S10)-(S12). Moreover, in the synchronized state the temporal translational symmetry (TTS) is preserved because both the amplitudes and phase difference of two cavity modes remain invariant, while the TTS is broken in the unsynchronized and limit cycle states. Here we demonstrate that these long-term states have different trajectories and topologies by introducing the following transform

$$x = \frac{1}{\sqrt{2}}(r_1 + r_2) \cos(\phi), \quad (\text{S13})$$

$$y = \frac{1}{\sqrt{2}}(r_1 + r_2) \sin(\phi), \quad (\text{S14})$$

$$z = \frac{1}{\sqrt{2}}(r_1 - r_2). \quad (\text{S15})$$

Figure S1 shows the mapping from the orthogonal space (r_1, r_2, ϕ) into the transformed space (x, y, z) with $x^2 + y^2 > z^2$. In this transformed space, the regions within the upper and lower cones are forbidden, while the points with the same z coefficient on the cone surface are topologically adhered [S2].

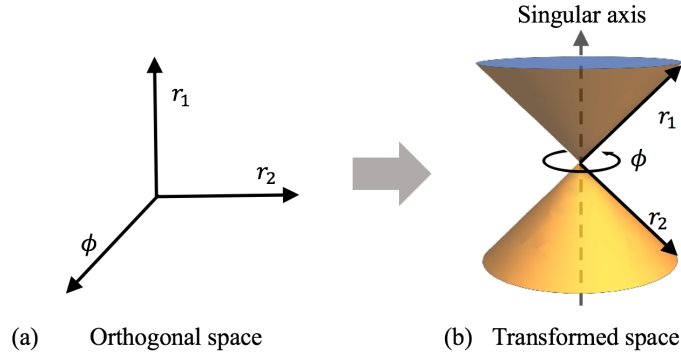


FIG. S1: (a) Orthogonal space (r_1, r_2, ϕ) . (b) The transformed space (x, y, z) with a clear topological structure. The dashed axis stands for the singular axis in this transformed space.

In Fig. S2, the long-term trajectories of three different states are plotted. As shown in Fig. S2(a), the unsynchronized trajectory encircles the singular axis ($x = y = 0$) of the transformed space (x, y, z) , while the synchronized and limit cycle trajectories do not [see Figs. S2(b) and S2(c) respectively]. These mean that these three states have different topologies. To show this, a character number χ is defined to be the average loops encircling the axis each period [S2], i.e.,

$$\chi = \frac{T_0}{2\pi} \lim_{T \rightarrow \infty} \left| \frac{1}{T} \int_0^T dt (\omega_1 - \omega_2) \right|. \quad (\text{S16})$$

The axis in the main text is represented by the cross in Fig. 2a3-c3 as equivalent projection of the singular axis here in transformed x-y plane, and the character number Eq. (3) in main text shares the meaning and form in this section. Numerical simulation shows that the synchronized trajectory has the character number $\chi = 2\pi$, while it becomes $\chi = 0$ in both the synchronized and limit cycle trajectories. According to the different symmetries and topologies, the three long-term states are classified as shown in the Table I.

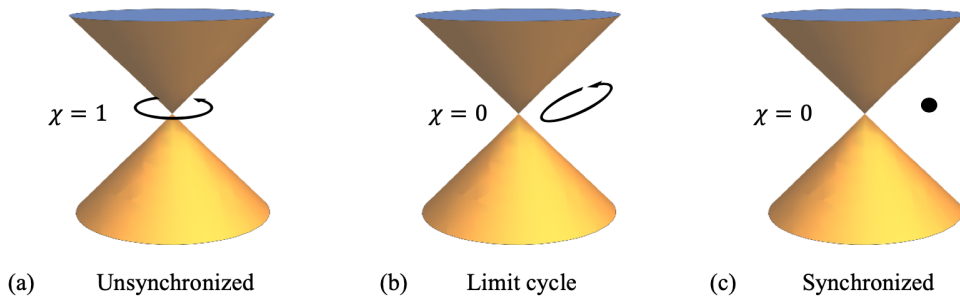


FIG. S2: Trajectories for the uncynchronized (a), limit cycle (b) and synchronized (c) states in the transformed space, with the corresponding character numbers χ .

Supplementary Table I: Classification of the different long-term states

State	TTS	Character number χ
Unsynchronized	Broken	1
Limit Cycle	Broken	0
Synchronized	Unbroken	0

III. NOISE ANALYSIS

The second and third order terms in Eq. (S4) denote the noisy motion in the phase space. Here we consider the leading second order term (in orders of A^{-2}) to demonstrate how synchronization affects the background noises. By introducing the frequency domain noisy operators $n_1(\omega)$ and $n_2(\omega)$, which satisfy,

$$\begin{pmatrix} n_1(\omega) \\ n_2(\omega) \\ n_1^\dagger(\omega) \\ n_2^\dagger(\omega) \end{pmatrix} \begin{pmatrix} n_1(\omega) & n_2(\omega) & n_1^\dagger(\omega) & n_2^\dagger(\omega) \end{pmatrix} \propto \mathbf{D}(\mathbf{\Lambda}_s, \bar{\mathbf{\Lambda}}_s), \quad (\text{S17})$$

the evolutions of the response operators $\delta a_1(\omega)$ and $\delta a_2(\omega)$ around the synchronized state are

$$\left[\frac{\partial \mathbf{f}(\mathbf{\Lambda}, \bar{\mathbf{\Lambda}})}{\partial(\mathbf{\Lambda}, \bar{\mathbf{\Lambda}})} + i\omega I - i\omega_s \underbrace{\begin{pmatrix} 1 & 0 \\ 0 & 1 \\ & -1 & 0 \\ & 0 & -1 \end{pmatrix}}_{\eta} \right] \begin{pmatrix} \delta a_1 \\ \delta a_2 \\ \delta a_1^\dagger \\ \delta a_2^\dagger \end{pmatrix} = \begin{pmatrix} n_1 \\ n_2 \\ n_1^\dagger \\ n_2^\dagger \end{pmatrix}. \quad (\text{S18})$$

Here ω_s is the frequency of the synchronized mode. Such approximation can also be applied in the unsynchronized and limit cycle states. Thus, the total responsive noise spectrum intensity

$$\begin{pmatrix} \delta a_1^\dagger & \delta a_2^\dagger & \delta a_1 & \delta a_2 \end{pmatrix} \begin{pmatrix} \delta a_1 \\ \delta a_2 \\ \delta a_1^\dagger \\ \delta a_2^\dagger \end{pmatrix} = (n_1^\dagger, n_2^\dagger, n_1, n_2) \left[\frac{\partial \mathbf{f}(\mathbf{\Lambda}, \bar{\mathbf{\Lambda}})}{\partial(\mathbf{\Lambda}, \bar{\mathbf{\Lambda}})} + i\omega I - i\omega_s \eta \right]^{-1\dagger} \left[\frac{\partial \mathbf{f}(\mathbf{\Lambda}, \bar{\mathbf{\Lambda}})}{\partial(\mathbf{\Lambda}, \bar{\mathbf{\Lambda}})} + i\omega I - i\omega_s \eta \right]^{-1} \begin{pmatrix} n_1 \\ n_2 \\ n_1^\dagger \\ n_2^\dagger \end{pmatrix}. \quad (\text{S19})$$

The resonance is achieved when the eigenvalues of $\partial \mathbf{f}(\mathbf{\Lambda}, \bar{\mathbf{\Lambda}})/\partial(\mathbf{\Lambda}, \bar{\mathbf{\Lambda}})$ has the same imaginary part $\omega_F = \omega \pm \omega_s$. The synchronized state achieved through different transitions has difference background noise distribution. In a first-order transition, $\omega_F = 0$ and the resonance is achieved exactly at the synchronization frequency ω_s . However, in a second-order transition, $\omega_F \neq 0$ and the resonance is shifted from ω_s at $\pm \omega_F$, as plotted in Fig. 1d of the main text. For the limit cycle state $\tilde{g} \approx \tilde{g}_c$ in Fig. 1c, the limit cycle mode is exited with a large amplitude. In the unsynchronized regime like $\tilde{g} \approx 0$, the modes are in the stand-alone oscillation. The noise intensity is the direct superposition of individual oscillators, as shown in Fig. 1b.

IV. THE DYNAMICAL POTENTIAL AND PHASE TRANSITION

The realization of the synchronized state requires both the existence and stability of a fixed point governed by the Eqs. (S10)-(S12). The fixed point always exists according to

$$f_1 = -r_1^3 + r_1 - \tilde{g}r_2 \sin(\phi) = 0, \quad (\text{S20})$$

$$f_2 = -r_2^3 + r_2 + \tilde{g}r_1 \sin(\phi) = 0, \quad (\text{S21})$$

$$f_3 = -\tilde{\Delta} - \tilde{\delta}(r_1^2 - r_2^2) - \tilde{g} \frac{r_2^2 - r_1^2}{r_1 r_2} \cos(\phi) = 0. \quad (\text{S22})$$

The stability requires the fixed point to be robust against perturbation, which relies on the local divergence of the trajectories. To analyze the divergence near the fixed point, a real-value dynamical potential $V(\mathbf{\Lambda}, \bar{\mathbf{\Lambda}})$ is defined as

$$\nabla^\dagger \cdot \nabla V(\mathbf{\Lambda}, \bar{\mathbf{\Lambda}}) = -\nabla \cdot \mathbf{f}(\mathbf{\Lambda}, \bar{\mathbf{\Lambda}}). \quad (\text{S23})$$

According to Eq. (S9), the change of the dynamical potential near the arbitrary point $(\mathbf{\Lambda}, \bar{\mathbf{\Lambda}})$ is given by

$$V(\mathbf{\Lambda} + \Delta\mathbf{\Lambda}, \bar{\mathbf{\Lambda}} + \Delta\bar{\mathbf{\Lambda}}) - V(\mathbf{\Lambda}, \bar{\mathbf{\Lambda}}) \approx -\frac{1}{2}(\Delta\bar{\mathbf{\Lambda}}, \Delta\mathbf{\Lambda}) \cdot \mathbf{f}(\mathbf{\Lambda} + \Delta\mathbf{\Lambda}, \bar{\mathbf{\Lambda}} + \Delta\bar{\mathbf{\Lambda}}) - \frac{1}{2}\mathbf{f}^\dagger(\mathbf{\Lambda} + \Delta\mathbf{\Lambda}, \bar{\mathbf{\Lambda}} + \Delta\bar{\mathbf{\Lambda}}) \cdot (\Delta\bar{\mathbf{\Lambda}}, \Delta\mathbf{\Lambda})^\dagger, \quad (\text{S24})$$

which is $-d(\Delta\mathbf{\Lambda} \cdot \Delta\mathbf{\Lambda}^\dagger)/dt$ in other words. In the vicinity of the fixed point $(\mathbf{\Lambda}_s, \bar{\mathbf{\Lambda}}_s)$,

$$V(\mathbf{\Lambda}_s + \Delta\mathbf{\Lambda}, \bar{\mathbf{\Lambda}}_s + \Delta\bar{\mathbf{\Lambda}}) = V(\mathbf{\Lambda}_s, \bar{\mathbf{\Lambda}}_s) - \frac{1}{2} [(\Delta\bar{\mathbf{\Lambda}}, \Delta\mathbf{\Lambda}) \cdot \mathbf{J} \cdot (\Delta\bar{\mathbf{\Lambda}}, \Delta\mathbf{\Lambda})^\dagger + \text{H.c.}] + \dots, \quad (\text{S25})$$

where $\mathbf{J} = \partial \mathbf{f}(\mathbf{\Lambda}, \bar{\mathbf{\Lambda}}) / \partial (\mathbf{\Lambda}, \bar{\mathbf{\Lambda}})$ stands for the Jacobi matrix. A stable fixed point requires $-d(\Delta \mathbf{\Lambda}^\dagger \cdot \Delta \mathbf{\Lambda}) / dt < 0$ for any small perturbation $\Delta \mathbf{\Lambda}$, which means that the fixed point has to be the local minimum of the dynamical potential. Equation (S25) shows that the distribution of the dynamical potential near the fixed point is explicitly given by the eigenvalues of \mathbf{J} together with its eigenvectors. The most important parameter affiliated to \mathbf{J} is the largest Lyapunov exponent \mathcal{L} , as the largest real part among the eigenvalues of \mathbf{J} [S3]. The local minimum is realized only if $\mathcal{L} < 0$.

As is achieved in Eq. (S10)-(S12), the total phase $\phi_1 + \phi_2$ is not involved in the evolution, thus \mathbf{J} always has a zero eigenvalue corresponding to $\phi_1 + \phi_2$. For the rest parameters (r_1, r_2, ϕ) , the reduced Jacobian matrix \mathbf{J}_R is defined as

$$\begin{pmatrix} \delta \dot{r}_1 \\ \delta \dot{r}_2 \\ \delta \dot{\phi} \end{pmatrix} = \mathbf{J}_R(r_1, r_2, \phi) \begin{pmatrix} \delta r_1 \\ \delta r_2 \\ \delta \phi \end{pmatrix}, \quad (\text{S26})$$

where

$$\mathbf{J}_R(r_1, r_2, \phi) = \begin{pmatrix} \frac{\partial f_1}{\partial r_1} & \frac{\partial f_1}{\partial r_2} & \frac{\partial f_1}{\partial \phi} \\ \frac{\partial f_2}{\partial r_1} & \frac{\partial f_2}{\partial r_2} & \frac{\partial f_2}{\partial \phi} \\ \frac{\partial f_3}{\partial r_1} & \frac{\partial f_3}{\partial r_2} & \frac{\partial f_3}{\partial \phi} \end{pmatrix}. \quad (\text{S27})$$

It is easily verified that \mathbf{J}_R is a projected representation of the global \mathbf{J} in the subspace, and thus has the same non-zero eigenvalues as \mathbf{J} . This means that the fundamental properties of the dynamical potential can be revealed by studying \mathbf{J}_R .

As \mathbf{J}_R has purely real components, its eigenvalues would be all real values or one real value with a pair of conjugated solution. Let the eigenvalues of \mathbf{J}_R be l_1, l_2 and $\text{Re}(l_1) \geq \text{Re}(l_2) \geq \text{Re}(l_3)$, and the basis vectors \mathbf{e}_i are defined to be the l_i -eigenvectors. In this case, the dynamical potential is transformed to the following quadratic form,

$$V = - \sum_{i=1,2,3} \text{Re}(l_i) |x_i|^2, \quad (\text{S28})$$

$$x_i = \mathbf{e}_i \cdot \mathbf{\Omega} \begin{pmatrix} \Delta \mathbf{\Lambda}^\top \\ \Delta \bar{\mathbf{\Lambda}}^\top \end{pmatrix}, \quad (\text{S29})$$

where $\mathbf{\Omega}$ corresponds to the projection matrix from the normal frame and $(\mathbf{\Lambda}, \bar{\mathbf{\Lambda}})$ is here defined in the frame spanned by $\mathbf{e}_1, \mathbf{e}_2$ and \mathbf{e}_3 . Near the transition point $\mathcal{L} = 0$, there exists two cases of the eigenvalues,

$$l_1 = \begin{cases} \mathcal{L} > \text{Re}(l_2) \geq \text{Re}(l_3), & \text{case I} \\ \mathcal{L} + i\omega_F = \bar{l}_2, \text{ and } \mathcal{L} > \text{Re}(l_3), & \text{case II} \end{cases}. \quad (\text{S30})$$

For the case I given that $\mathcal{L} = b_0(\tilde{g}_c - \tilde{g})$, where $b_0 = -d\mathcal{L}(\mathbf{\Lambda}_s(\tilde{g}), \bar{\mathbf{\Lambda}}_s(\tilde{g})) / d\tilde{g} > 0$, we simplify the dynamical potential in Eq. (S25) as

$$V = -b_0(\tilde{g}_c - \tilde{g})x_1^2 - \underbrace{\text{Re}(l_2)|x_2|^2 - \text{Re}(l_3)|x_3|^2}_{\text{Positive definite part}}. \quad (\text{S31})$$

Here x_1 coincides with x defined in Eq. (5) in the main text, and the coefficient b_0 is the same. Now that the eigenvalue is purely real, the displacement grows exponentially along the direction of eigenvector with $\tilde{g} < \tilde{g}_c$, which indicates the emergence of the unsynchronized state. Judging from the dynamical potential in Eq. (S31), the transition from the synchronized state to the unsynchronized state is of first-order at \tilde{g}_c .

For the case II, the conjugated pair (l_1, l_2) always has the same real part and the instability onsets in the $(\mathbf{e}_1, \mathbf{e}_2)$ plane. At the transition point $\mathcal{L} = 0$, a series of periodic solutions are written as

$$\begin{pmatrix} \rho \cdot e^{i\omega_F t} \\ \rho \cdot e^{-i\omega_F t} \\ 0 \end{pmatrix} = \mathbf{\Omega} \begin{pmatrix} \Delta \mathbf{\Lambda}^\top \\ \Delta \bar{\mathbf{\Lambda}}^\top \end{pmatrix}, \quad (\text{S32})$$

where $\rho = \sqrt{|x_1|^2 + |x_2|^2}$ stands for the variable radius of the perturbation circle and $\omega_F > 0$ without loss of generality. The dynamical potential here just describes the expansion property of trajectories while the rotational information is eliminated. Different from the former one-dimensional case where the largest Lyapunov exponent corresponds to a purely real eigenvalue, it should be calculated along the circular trajectory as a correction to the incomplete information of argument. The temporal averaging correction is done by integration [S4]

$$\langle V \rangle = \frac{\omega_F}{2\pi} \int_0^{2\pi/\omega_F} dt V(\mathbf{\Lambda}_{\text{circle}}, \bar{\mathbf{\Lambda}}_{\text{circle}}), \quad (\text{S33})$$

where

$$(\mathbf{\Lambda}_{\text{circle}}, \bar{\mathbf{\Lambda}}_{\text{circle}})^\top = \mathbf{\Omega}^{-1} \begin{pmatrix} \rho \cdot e^{i\omega_F \tau} \\ \rho \cdot e^{-i\omega_F \tau} \\ 0 \end{pmatrix}. \quad (\text{S34})$$

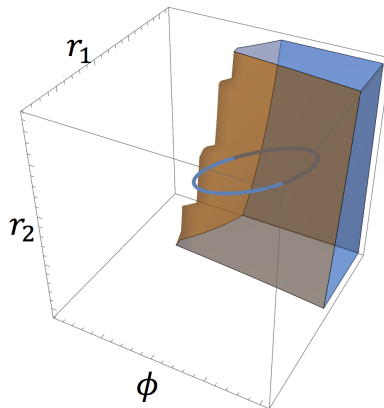


FIG. S3: The zoomed-in view of limit cycle in the orthogonal space (r_1, r_2, ϕ) . The stable region $\mathcal{L} < 0$ is shaded. The limit cycle is across the boundary in agreement with the reduced two-dimensional motion. The factors $b_1 = 0.00437246$ and $b_2 = -0.0234752$ are calculated in verification of the theory presented in the text.

With $\mathbf{e}_1/\sqrt{2} + i\mathbf{e}_2/\sqrt{2}$, $\mathbf{e}_1/\sqrt{2} - i\mathbf{e}_2/\sqrt{2}$ and \mathbf{e}_3 as the basis vectors, the reduced Jacobian has a diagonal block

$$\mathbf{J}_R = \begin{pmatrix} \mathcal{L} & \omega_F & 0 \\ -\omega_F & \mathcal{L} & 0 \\ 0 & 0 & l_3 \end{pmatrix}. \quad (\text{S35})$$

When the coupling strength $\tilde{g} \approx \tilde{g}_c$, $\mathcal{L} \propto (\tilde{g}_c - \tilde{g})$ and $\mathcal{L} \ll \omega_F$. Further expansion into the higher-order term is performed with

$$\mathcal{L} = b_0(\tilde{g}_c - \tilde{g}) + \sum_{i=1,2,3} x_i \frac{\partial \mathcal{L}}{\partial x_i} + \sum_{i,j=1,2,3} \frac{1}{2} x_i x_j \frac{\partial^2 \mathcal{L}}{\partial x_i \partial x_j}. \quad (\text{S36})$$

The diagonal part $\begin{pmatrix} \mathcal{L} & 0 \\ 0 & \mathcal{L} \end{pmatrix}$ as arbitrary small perturbation against $\begin{pmatrix} 0 & \omega_F \\ -\omega_F & 0 \end{pmatrix}$ can be separated, and the averaging correction in the radial direction ρ is given by

$$\langle V \rangle = -\frac{\omega_F}{2\pi} \int_0^{2\pi/\omega_F} d\tau \begin{pmatrix} \rho \sin(\omega_F \tau) & \rho \cos(\omega_F \tau) \end{pmatrix} \begin{pmatrix} \mathcal{L} & 0 \\ 0 & \mathcal{L} \end{pmatrix} \begin{pmatrix} \rho \sin(\omega_F \tau) \\ \rho \cos(\omega_F \tau) \end{pmatrix}. \quad (\text{S37})$$

Combining Eq. (S36) and Eq. (S37), the averaged dynamical potential is expanded as

$$\langle V \rangle = -\frac{\omega_F}{2\pi} b_0 (\tilde{g}_c - \tilde{g}) \rho^2 + \frac{\omega_F}{8\pi} \left(\frac{\partial^2 \mathcal{L}}{\partial x_1^2} + \frac{\partial^2 \mathcal{L}}{\partial x_2^2} \right) \rho^4. \quad (\text{S38})$$

Equation (S38) gives out the form of Eq. (6) in the main text by redefining $b_1 = \omega_F b_0 / 2\pi$ and $b_2 = \omega_F (\partial^2 \mathcal{L} / \partial x_1^2 + \partial^2 \mathcal{L} / \partial x_2^2) / 8\pi$. As long as $b_2 < 0$ is satisfied, the double-well type potential is achieved, presenting a second-order transition at the critical point \tilde{g}_c . When $\tilde{g} < \tilde{g}_c$ and $b_2 > 0$, the radial displacement stops growth at the shifted minimum as a result of the double well, which corresponds to the generation of the limit cycle state. For demonstration, the limit cycle of the orthogonal space (r_1, r_2, ϕ) is plotted in Fig. S3, when $\tilde{\Delta} = 0.3$, $\tilde{\delta} = 0.1$ and $\tilde{g} = 0.398$. The trajectory balances near the boundary between the stable and the unstable regions. The averaged dynamical potential in the vicinity of the fixed point $r_1 = 0.651228$, $r_2 = 1.09682$, $\phi = 2.10801$ is calculated according to Eq. (S38) with $b_1 = 0.00437246$ and $b_2 = -0.0234752$.

During different types of transitions, the behaviors of the topological character are distinct. In the first-order transition [see Fig. S4(a)], the topological character number χ is variant due to the drastic transition between a fixed point and a trajectory encircling the singular axis. In the second-order transition [see Fig. S4(b)], the gradual expansion and contraction of limit cycle promise the invariant χ , because both the arbitrarily small limit cycle and the fixed point do not encircle the singular axis.

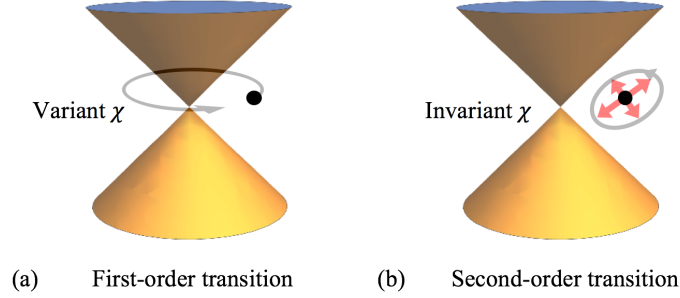


FIG. S4: Topological character is variant or invariant during the first-order (a) or the second-order (b) transition.

V. HYSTERESIS BEHAVIOR

The hysteresis process is realized by varying the coupling strength at an extremely slow rate with different $(\tilde{\Delta}, \tilde{\delta})$. The emergence of the frequency locking under the critical coupling strength can be explained via the following equation

$$(\dot{\Lambda}_s + \Delta\dot{\Lambda}, \dot{\tilde{\Lambda}}_s + \Delta\dot{\tilde{\Lambda}}) = \mathbf{f}(\Lambda_s + \Delta\Lambda, \tilde{\Lambda}_s + \Delta\tilde{\Lambda}). \quad (\text{S39})$$

Its second-order temporal derivation is given by

$$(\ddot{\Lambda}_s + \Delta\ddot{\Lambda}, \ddot{\tilde{\Lambda}}_s + \Delta\ddot{\tilde{\Lambda}}) = (\dot{\Lambda}_s + \Delta\dot{\Lambda}, \dot{\tilde{\Lambda}}_s + \Delta\dot{\tilde{\Lambda}}) \cdot \frac{\partial \mathbf{f}}{\partial \Lambda} + \dot{g} \frac{\partial \mathbf{f}}{\partial \tilde{g}} \Big|_{\Lambda_s + \Delta\Lambda}, \quad (\text{S40})$$

which is further simplified as

$$(\Delta\ddot{\Lambda}, \Delta\ddot{\tilde{\Lambda}}) - (\Delta\dot{\Lambda}, \Delta\dot{\tilde{\Lambda}}) \cdot \frac{\partial \mathbf{f}}{\partial \Lambda} - \dot{g} \left(\frac{d}{d\tilde{g}} \frac{\partial \mathbf{f}}{\partial \Lambda} \right) \Delta\Lambda = -(\ddot{\Lambda}_s, \ddot{\tilde{\Lambda}}_s). \quad (\text{S41})$$

Equation (S41) is a perturbed linear differential equation, which can be solved by eigenvalue analysis of the matrix $M = \frac{d}{d\tilde{g}} \frac{\partial \mathbf{f}}{\partial \Lambda}$, i.e.,

$$\text{Det}(\lambda^2 \mathbf{I} - \lambda \mathbf{J} - \dot{g} M) = 0. \quad (\text{S42})$$

With the assumption in Sec. IV, $M = -b_0 \mathbf{I}$. In the $(\mathbf{e}_1/\sqrt{2} + i\mathbf{e}_2/\sqrt{2}, \mathbf{e}_1/\sqrt{2} - i\mathbf{e}_2/\sqrt{2})$ plane, Eq. (S42) is explicitly simplified as

$$\begin{vmatrix} \lambda^2 + b_0(\tilde{g}_c - \tilde{g})\lambda + \dot{g}b_0 & -\omega_F\lambda \\ \omega_F\lambda & \lambda^2 + b_0(\tilde{g}_c - \tilde{g})\lambda + \dot{g}b_0 \end{vmatrix} = 0. \quad (\text{S43})$$

When $\dot{g}_c \neq 0$, two non-zero eigenvalues

$$\lambda_{\pm} = \frac{\dot{g}b_0}{b_0^2(\tilde{g}_c - \tilde{g})^2 + \omega_F^2} [b_0(\tilde{g}_c - \tilde{g}) \pm i\omega_F], \quad (\text{S44})$$

which can be easily approached with the eigenvalues of $-\dot{g}\mathbf{J}_R^{-1}M$ by eliminating the λ^2 term in Eq. (S42) (the decoupled degree $\phi_1 + \phi_2$ is not involved in this process and here \mathbf{J}_R instead of \mathbf{J} in Eq. (S25) gives the perturbed eigenvalues).

Equation (S43) has two solutions $\lambda_{\pm} = 0$, which do not work at $\dot{g} = 0$. When $\omega_F = 0$ and $\dot{g} \neq 0$, the transition is of first-order, and λ_{\pm} go divergent as a result of the singularity of \mathbf{J}_R^{-1} at the point $\tilde{g}_c = \tilde{g}$ in Eq. (S44). At $\tilde{g} = \tilde{g}_c$,

λ_{\pm} jump from $+\infty$ to $-\infty$ in both the forward and backward trips. Thus the synchronization is always drastic at $\tilde{g} = \tilde{g}_c$ for arbitrary small \tilde{g} . When $\omega_F \neq 0$ and $\tilde{g} \neq 0$, the transition is of second-order, and in both the trips the real parts of λ_{\pm} transit from $+\epsilon$ to $-\epsilon$ at \tilde{g}_c , where ϵ is an infinitesimal. In the forward trip, the trajectories are far from the fixed point $\mathbf{\Lambda}_s$, and λ_{\pm} will not be involved in the dynamics until the synchronization is achieved. However, in the backward trip, the dynamics switch into the branch governed by λ_{\pm} from the fixed point $\mathbf{\Lambda}_s$. A hysteresis loop is finally generated due to the switching of different branches [S5].

-
- [S1] H. Carmichael, *Statistical Methods in Quantum Optics 1: Master Equations and Fokker-Planck Equations* (Springer, 1999).
[S2] M. A. Armstrong, *Basic topology* (Springer Science & Business Media, 2013).
[S3] A. M. Lyapunov, *Int. J. Control* **55**, 531 (1992).
[S4] J. E. Marsden and M. McCracken, *The Hopf bifurcation and its applications*, vol. 19 (Springer Science & Business Media, 2012).
[S5] N. Berglund, *Prog. Theor. Phys. Suppl.* **139**, 325 (2000).